High power density and bias-free reverse electrowetting energy harvesting using surface area enhanced porous electrodes

Pashupati R. Adhikari [a,*], Russell C. Reid [b], Ifana Mahbub [c]

[a] Department of Mechanical Engineering, University of North Texas, Denton, TX, 76207, USA
[b] Department of Engineering, Dixie State University, St. George, UT, 84770, USA
[c] Department of Electrical Engineering, University of North Texas, Denton, TX, 76207, USA

HIGHLIGHTS

- Low frequency (1–5 Hz) motion energy harvesting using high surface area electrodes.
- Highest reported REWOD power density (4.8 $\mu W/cm^2$) without bias voltage.
- Experimentally supported capacitive theoretical modeling.
- Demonstration of increasing power density with shrinking pore size electrodes.
- Power density increased by ~23 times compared to planar electrodes.

GRAPHICAL ABSTRACT
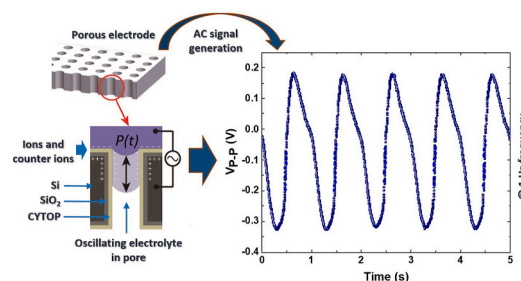
ARTICLE INFO

ABSTRACT

Reverse electrowetting-on-dielectric (REWOD) is a novel energy harvesting technology with a significant advantage over other energy harvesting technologies due to its effective performance at a low-frequency range and not requiring resonance frequency of solid structures. However, REWOD energy harvesting based on planar electrodes has a limited surface area and therefore a lower power output. In this work, we present a novel approach for enhancing power output from a REWOD energy harvester by significantly increasing the total available surface area using perforated silicon wafer electrodes. Without applying any external bias voltage, maximum current and voltage densities per unit planar area were measured to be 3.77 $\mu A/cm^2$ and 1.05 V/cm^2, respectively, for a 38 μm pore-size electrode at 5 Hz modulation frequency. RMS power density output was 4.8 $\mu W/cm^2$, which is ~23 times higher than that from our prior work on planar electrodes showing the significance of porous electrodes in REWOD energy harvesting. A simple capacitive theoretical model validating experimental results was developed and justified. The novelty of this work lies in the combination of a bias-free approach to REWOD energy harvesting coupled with significant enhancement in electrode surface area per planar area to increase the output power density.

---

* Corresponding author. Department of Mechanical Engineering, University of North Texas, Discovery Park, 3940 N Elm St, Suite F115, Denton, TX, 76207, USA.
E-mail address: pashupatiadhikari@my.unt.edu (P.R. Adhikari).

1. Introduction

Manipulating a liquid droplet with an applied electrical field has long been studied and is known as electrowetting-on-dielectric (EWOD). In recent years, a new approach to energy harvesting that is related to EWOD has been demonstrated and it is termed as reverse electrowetting-on-dielectric (REWOD) energy harvesting [1,2]. In REWOD, the kinetic energy of liquid motion is converted into electrical energy as a liquid droplet is periodically deformed between two dielectrically coated electrodes under the application of an external mechanical force, inducing a periodic change in electrode-electrolyte interfacial area. This periodic change in the interfacial area induces a change in the electrical capacitance at the liquid-solid interface and forces electrical current to flow back and forth across a load resistor to generate electrical power. For low frequency motion activities such as walking and running, REWOD energy harvesting has been demonstrated to be advantageous compared to other existing energy harvesting technologies such as vibration-based electrostatic energy harvesting, electromagnetic energy harvesting, piezoelectric energy harvesting, and triboelectric nano-generators (TENGs) [3–7]. Unlike most energy harvesters with the exception of TENGs, REWOD energy harvesting is highly efficient at harvesting energy at lower frequencies (<10 Hz) and does not require resonance of solid structures. TENG has been demonstrated to efficiently perform at a low frequency range (0.25 Hz–5 Hz), which is the typical frequency range for several human motion activities [7,8]. However, TENGs generally require electrodes to undergo continuous solid-solid friction contributing to material deterioration, directly affecting the lifespan and reliability of the generators [9,10]. Even though efforts have been made to minimize the friction by introducing liquid and conductive cushioning materials in between electrodes, the underlying friction principle by which TENG operates, is unavoidable, thus imposing an obstacle to the reliability and longevity of this technology [11]. Hybrid-type TENG has also been reported with high power density. Wang et al. reported a hybrid type of energy harvester that works based on a combination of three different energy harvesting techniques: piezoelectric, electromagnetic, and TENG [12]. However, since all three energy harvesting techniques in principle work differently, it would not be very reliable, especially for the application of low frequency motion energy harvesting. REWOD works based on the principle of energy conversion from mechanical modulation of microliter volume of liquid droplets into electrical energy and does not require a resonance of solid structures. As a result, REWOD has an ability to directly utilize a very broad range of mechanical forces and displacements of microliter volume of liquid droplets into electrical energy unlike many other energy harvesters including TENG. In summary, a parametric comparison of various input parameters and output power densities of the energy harvesting technologies discussed above are presented in Table S1.

Much of the REWOD energy harvesting research reported to date have shown the efficacy of this energy harvesting technology to potentially power various electronics that are integral to our everyday life [13–15]. However, most, if not all, REWOD research have used DC bias-voltage as a means to push REWOD generated current through the electric circuit to power up electronics. The bias voltage ranged from few Volts to tens of Volts, which directly increase the power density as compared to energy harvesters without bias voltage [1,2,13,15]. The concept of energy harvesting as a means to replace batteries or external bias sources then becomes compromised. In order to fully self-power electronics, the device should be battery/bias source free and be able to fully power-up the electronics. In addition, using a battery in an energy harvester is disadvantageous due to battery size, weight, and limited lifetime, asserting an obstacle to the modern design conception of mobility and sustainability. For this reason, we have taken the bias-free approach, using deionized water electrolyte as charge carriers, without the need for any external bias-voltage for REWOD energy harvesting. Note that the industrial grade DI water in its pure form is highly polar with very high resistance (~18.2 MΩ-cm) and cannot be used as

charge carriers. However, when exposed to an open environment (laboratory setting), the DI water quickly absorbs impurities that significantly lowers its resistance making it a possible electrolyte [14]. In addition, as a novelty of this work, the available surface area per planar area of the electrodes is significantly increased making the energy harvester ideal for miniaturized electronic devices. Since wearable and implantable electronics in human health monitoring have greatly miniaturized over the years, the available surface area has become limited [16–19]. Our approach of REWOD energy harvesting with high surface area porous electrodes can overcome the challenges in these efforts by yielding high power density.

The amount of current generation in REWOD primarily depends on the interfacial contact area between electrodes and electrolyte. Other important parameters include the dielectric material and thickness, surface charge density, and modulation frequency. These parameters directly or indirectly influence the capacitance in the dielectric material and therefore they also affect the AC current generation from the energy harvester. In our prior work involving planar electrodes, we explored an optimization route by configuring various combination of such parameters and demonstrated the feasibility of enhancing power density [20]. Increased current and power density was demonstrated using higher frequency modulation of electrolytes with higher molarity, thinner dielectric film of materials with higher dielectric constants, all in the absence of bias voltage. Accordingly, prior REWOD research has been focused on the use of planar electrodes which limits the interfacial area [13,20–22]. One way to increase the interfacial area is by increasing the number of electrolyte droplets [14,23,24]. However, the idea of increasing the interfacial contact surface area per unit planar area and hence increasing the current output is not limited to the number of fluidic droplets on planar electrodes. As proposed herein, another approach for increasing surface area is to use porous materials with high pore depth-to-diameter aspect ratio.

One of the key parameters in this work that dictates electrolyte insertion and retraction to achieve maximum power density is the pulsating pressure. A pressure-based theoretical model showing a relationship between the solution of the Washburn equation and the associated electrical power generation has been previously reported, but no experimental work was performed to validate the model [25]. The Washburn equation describes the time-rate of pore filling with an electrolyte under a time-dependent pulsating pressure, $P(t)$ [26]. Prins et al. demonstrated fluid electroactuation wherein an applied voltage was used to control electrocapillary pressure in microchannels [27]. They predicted that smaller microchannel diameters lead to a higher pressure. A microhydraulic electrowetting actuator was demonstrated by Kedzierski et al. [28]. Their pioneering work focused on a capacitive energy conversion device using capillary pressure and electrowetting to reversibly convert electrical power to hydraulic power for micro-robotics and energy harvesting applications. Our work focuses on generating energy simply by applying pulsating pressure to generate AC voltage through interaction between high surface area porous electrodes and electrolyte and hence generate maximum power output *without any applied bias source.*

The working mechanism of the high surface area REWOD energy harvesting, where AC voltage is generated by inserting and retracting liquid electrolyte in and out of micro-pores using pulsating pressure is illustrated in Fig. 1(a)-(b). Time variant pulsating pressure, $P(t)$, at a given frequency is applied to insert and retract liquid electrolyte in and out of the micro-pore of the high surface area porous electrode. A periodic change in electrode-electrolyte interfacial area results in changing capacitance with respect to time and generates AC voltage.

In this work, we have successfully generated AC power through REWOD energy harvesting using high surface area porous electrodes that we have fabricated. A device that can generate pulsating pressure was designed to insert and retract liquid electrolyte in and out of the pores. With precise control of the device, AC voltage was generated for a frequency range of 1–5 Hz with 0.5 Hz step. The original contributions of
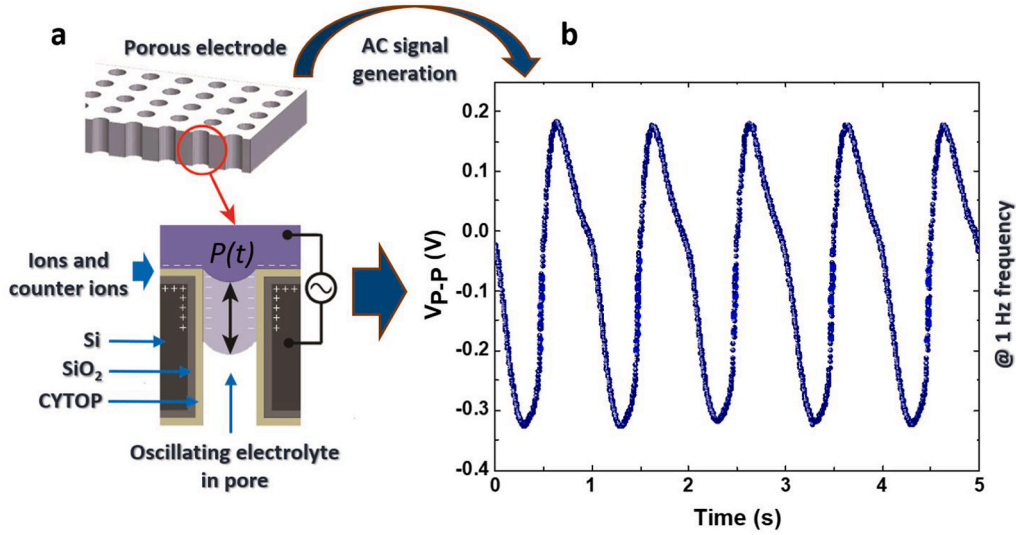
Fig. 1. (a) Working mechanism of high surface area reverse electrowetting energy harvesting with pulsating pressure, *P(t)*. (b) Generation of REWOD AC voltage.

this work are summarized as follows: (1) the fabrication and implementation of various porous electrodes to demonstrate high surface area REWOD-based energy harvesting, (2) an analytical capacitive model validating the experimental results that can be used to maximize the REWOD energy harvester's power density, and (3) demonstration of AC voltage and current generation using pulsating pressure. REWOD energy harvesting without applied bias voltage using enhanced surface area porous electrodes and demonstration of the highest power density among REWOD works without bias voltage is the innovative aspect of this work. The proposed REWOD energy harvesting system and the approach we have taken in this work is highly efficient and can generate ~23 times the RMS power density at 5 Hz modulation frequency compared to that of a planar electrode approach from our prior work [20]. At 3 Hz modulation frequency, the power density from this work is well enhanced from our previous work on planar electrodes (~8 times) and could be further improved considering a higher surface area material such as denser pores or conductive porous carbon materials. As part of a practical application of REWOD energy harvester, our recent work in implementing charge amplifier and DC-DC converter integration into the REWOD energy harvester can produce sufficient DC power at low frequency (<3 Hz) to self-power wearable motion sensors [29–31]. The charge that is being generated by the REWOD is recorded and amplified by the charge amplifier, digitized by the analog-to-digital converter (ADC), and the digitized data is transmitted by the transmitter wirelessly, making the REWOD a self-powered wireless motion sensor. Many devices such as glucose sensor, intraocular pressure monitor, and intraocular temperature monitor require power supply in the range of 0.27 μW–3 μW and a constant DC voltage of 1.2–1.5 V [32–35]. Our preliminary results show the capability of generating the range of power and voltage with implementation of highly efficient rectifier and voltage regulators.

2. Design and theoretical modeling

The REWOD harvester in this research is modeled as a capacitor consisting of conductive liquid electrolyte on one side, an insulating layer of a given thickness in the middle, and a conductive surface (doped Si) on the other side as shown in Fig. 1(a). The capacitance of this model is the combination of a constant capacitance and a time-varying capacitance due to how the electrolyte interacts with the electrodes. The constant capacitance C_C is due to the constant presence of electrolyte at the top planar surface of the electrode. The time varying capacitance $C(t)$ is due to the electrolyte insertion and retraction in and out of

the pores because of the application of pulsating pressure. Therefore, the total capacitance at the electrode-electrolyte interface, $C_P(t)$ can be modeled as shown in Equation (1):

$$C_P(t) = C_C + C(t) = \frac{\varepsilon_0 \varepsilon_r A_C}{d} + \frac{\varepsilon_0 \varepsilon_r A(t)}{d} \quad (1)$$

where, $\varepsilon_0 = 8.85 \times 10^{-12}$ F/m is the vacuum permittivity, ε_r is the relative permittivity of the dielectric material, d is the total thickness of the dielectric layers, A_C is the constant planar area, and $A(t)$ is the variable electrode-electrolyte interfacial area within the pores. The proposed theoretical model also includes a resistor R_P, and a current source $I_P(t)$ in parallel with the variable capacitor $C_P(t)$. Together, these represent the REWOD energy harvester, which, when placed in parallel with an external load resistance R_L, complete the equivalent circuit model shown in Fig. 2(a). The accompanying Fig. 2(b) shows a cross-section of a porous electrode to illustrate which portions of the electrode surface area give rise to C_C and $C(t)$. The dielectric layer thickness, d, depicted in the figure is the total thickness of the dielectric layer consisting of SiO$_2$ and a layer of CYTOP, which is a hydrophobic fluoropolymer commonly used in EWOD/REWOD. The permittivity, ε_r, given in Equation (1) is the effective relative permittivity of the SiO$_2$ and CYTOP, which can be calculated using Equation (2) [36]:

$$\varepsilon_{eff} = \frac{d_1 + d_2}{\frac{d_1}{\varepsilon_{r1}} + \frac{d_2}{\varepsilon_{r2}}} \quad (2)$$

where ϵ_{r1} and ϵ_{r2} are the relative dielectric constants of the hydrophobic layer (CYTOP) and dielectric layer (SiO$_2$), respectively and d_1 and d_2 are the thicknesses of CYTOP and SiO$_2$, respectively. Considering bulk material properties, the dielectric constants used in the calculation of the effective capacitance are: $\epsilon_{r1} = 2.1$, and $\epsilon_{r2} = 3.9$ [37]. A parallel arrangement in the electrical model was used rather than a series arrangement to eliminate the complexity of requiring two different voltages across the resistor and capacitor in the model. Additionally, many piezoelectric and pyroelectric energy harvesting models assume a parallel arrangement with the current source [38,39].

$I_P(t)$ represents generated AC REWOD current, which is the rate of change of generated charge across the REWOD electrodes. $C_P(t)$ acts as a variable capacitor that changes periodically during the electrolyte modulation while electrical resistance, R_P, occurs across the electrodes due to the electrical conductivity and thickness of the electrolyte, dielectric, and conductive layers along with the electrode-electrolyte interface. Thus, the resistance, R_P can be modeled as shown in Equation (3):
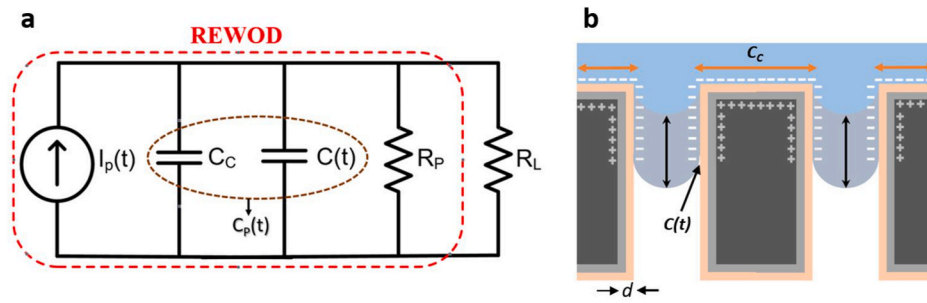
Fig. 2. (a) RC model of proposed REWOD energy harvester in parallel with a load resistance, R_L. (b) Schematic illustration showing the location on the porous electrode that give rise to C_C and $C(t)$.

$$R_P = \frac{\rho l}{A} \qquad (3)$$

where ρ is the resistivity, l is the total combined thickness of the conductive layer (doped Si), the dielectric layers (SiO$_2$ and CYTOP), and the electrolyte (DI water), and A is the electrode-electrolyte interfacial area.

The four different fabricated electrodes (later discussed in detail in the materials and fabrication section) have pore diameters of 38 μm, 50 μm, 76 μm, and 100 μm with a fixed pore depth of 380 μm (through the Si wafer). These pore parameters were chosen to achieve four different approximate pore-length-to-diameter (L/D) aspect ratios of 10, 8, 5, and 4, respectively. The pores are confined within a circular area of 3.14 cm^2 on the wafer surface (a circular area with 1 cm radius) and the number of pores varies with pore size diameter. In order to determine the total surface area available per planar area of 3.14 cm^2, assuming smooth pore sidewalls, we first calculated the side-wall surface area of a single pore using the equation for wall surface area of a cylinder as shown in Equation (4):

$$A = 2\pi r L \qquad (4)$$

where r is the pore radius and L is the pore length. The area of a single pore was then multiplied by the total number of pores to find the total area occupied by the pores. The planar portion of the surface area, A_C, was then determined by subtracting the pore cross-sectional areas from the total available planar area of 3.14 cm^2. Table 1 summarizes the planar area (A_C) and pore sidewall surface area (A_P) for each electrode with a different pore size, the total number of pores, and the total surface area enhancement due to the presence of pores.

The results from Table 1 shows that the surface area increases with the shrinking of the pore size since planar area, A_C, for each pore diameter are approximately the same. Theoretically, the surface area distribution in the table for the given electrodes likewise suggests that the electrodes with the smallest pore size would have the highest capacitance due to the direct proportionality between the capacitance and the surface area.

The effective dielectric permittivity, ε_{eff} from Equation (2), is calculated to be 2.73 using a total dielectric thickness, d of 200 nm (the thickness of the SiO$_2$ layer is 150 nm and the thickness of CYTOP layer is

~50 nm). Both components of the capacitance, C_C and $C(t)$, are calculated using Equation (1). The maximum theoretical capacitance assuming the electrolyte has fully covered the planar area as well as the entirety of the pore walls is given in Table 2. Referring to the constant area, A_C, in Table 1, the constant portion of the capacitance, C_C, in Table 2 for each pore size is almost identical and the only significant variation in capacitance is from $C(t)$, further validating the hypothesis that as the pore size decreases, the overall capacitance increases, primarily due to the increase in electrode-electrolyte interfacial area.
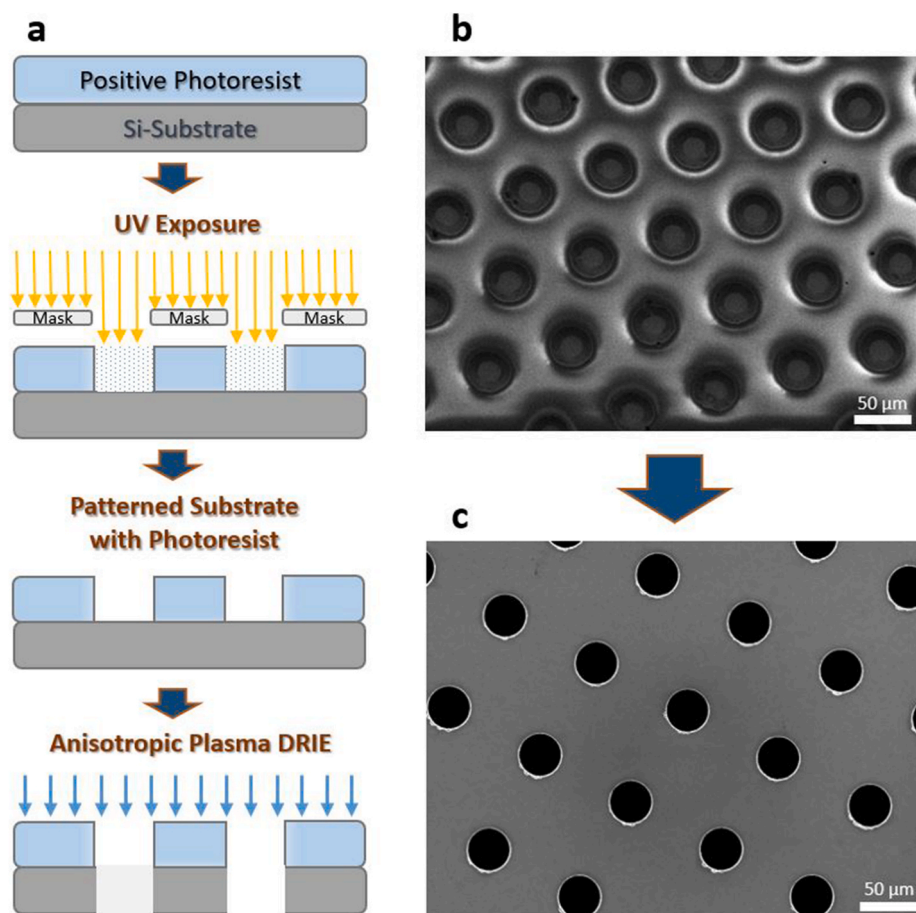
3. Experimental section

3.1. Materials and fabrication

A schematic of the high surface area porous electrode fabrication process is illustrated in Fig. 3(a). A very low resistance (0.001–0.005 Ω-cm), 100 mm diameter, 380 μm thick double side polished silicon wafer (University Wafers Inc.) was used to fabricate the porous samples with uniform pores. Si wafers were chosen as electrodes over metal electrodes because they are considered ideal for anisotropic plasma deep reactive ion etching (DRIE) to create uniform through pores. With metal electrodes, it would be very difficult to etch through-pores in micrometer (μm) scale. Each wafer sample had one of four different pore size patterns: 38 μm, 50 μm, 76 μm, and 100 μm in diameter, which were created using AutoCAD software within a circular area of 3.14 cm^2 (1 cm radius). High resolution chrome masks were created for each of the pore size patterns. A representative mask pattern for the 38 μm pores is shown in Fig. S1. KL6008 positive photoresist (Kemlab Inc.) was spin coated on the wafers with appropriate spin coating speed, soft-bake time, and temperature to achieve the desired photoresist thickness according to the photoresist data sheet. Prior to spin coating of the photoresist, wafers were cleaned with acetone and deionized water. The spin coating was performed at 300 rpm for 5 s (spread cycle) and 600 rpm for 45 s (spin cycle). This process provided a desired photoresist thickness of ~10–12 μm as required to protect the masked portion of the wafer during deep reactive ion etching (DRIE) later in the fabrication process. Wafers with photoresist were cured for 150 s at 105 °C on a hot plate. The cured wafers were exposed under the UV light for 45 s at 210 mJ/cm^2 of exposure broadband. Subsequently, the UV-exposed wafers were

Table 1
Summary of pore geometry and total surface area for four different electrodes that each have a different pore diameter.

Pore diameter (μm)	Number of pores	Planar area, A_C (cm^2)	Pore surface area, A_P (cm^2)	Total surface Area (cm^2)	Surface area enhancement (%)
38	51877	2.553	23.53	26.08	830
50	29701	2.558	17.73	20.29	646
76	12871	2.527	11.99	14.52	462
100	4681	2.774	5.59	8.36	266

Table 2
Pore geometry and their total capacitance showing constant planar capacitance and maximum porous capacitance assuming the electrolyte fully covers the entire pore length during modulation.

Pore diameter (μm)	Constant planar capacitance, C_C (μF)	Maximum pore capacitance, C_t (μF)	Total maximum capacitance, C_T (μF)
38	0.0363	0.3345	0.3708
50	0.0364	0.2520	0.2883
76	0.0359	0.1703	0.2062
100	0.0394	0.0794	0.1188

Fig. 3. (a) Steps involving fabrication process. (b) Patterned photoresist on Si-wafer using photolithography with ~10 μm thick positive photoresist. (c) Etched holes using plasma deep reactive ion etching (DRIE).

immediately developed using 0.26 N TMAH developer for ~2 min, rinsed with deionized water, and nitrogen air dried. The pore patterns and the photoresist thickness of the developed wafers were verified using Alpha-Step D-300 stylus profiler (KLA Corporation). A representative profilometer image of a fully patterned Si-wafer sample with photoresist is given in Fig. S2(a). Accompanying Fig. S2(b) shows the profilometer scan to verify the photoresist thickness of ~10 μm. An SEM image of a fully patterned Si-wafer with photoresist ready for DRIE is shown in Fig. 3(b).

The patterned wafers were etched to create through-pores using DRIE (Oxford 100 ICP) and deposited with SiO_2 dielectric using plasma CVD (Oxford Plasmalab 80). This process was completed at the University of Utah Nanofab. The anisotropic plasma DRIE was performed in the presence of sulfur hexafluoride (SF_6) at a flow rate of 80 sccm and octafluorocyclobutane (C_4F_8) at a flow rate of 90 sccm under a vacuum pressure of 7.5×10^{-9} torr. The wafers were cleaned by rinsing in xylene, acetone, xylene, and isopropanol in that order for 10 s each for several cycles. Rinsed wafers were then etched in piranha solution, rinsed, and dried for a complete removal of all the unwanted particles on the wafer surface during etching. Etched porous wafers were subsequently deposited with 150 nm of SiO_2 dielectric using plasma CVD. The thickness of the SiO_2 was verified using an optical profilometer (Zygo NewView 5000). Fig. 3(c) shows the etched porous Si-wafer after SiO_2 deposition (the variation in pore density in Fig. 3(b) and Fig. 3(c) is due to two different batches of electrode fabrication).

After SiO_2 deposition, the wafers were coated with an additional layer of hydrophobic material. A fluoropolymer, CYTOP (CTL-809 M), and its solvent (CT-Solv. 180), both purchased from AGC Chemicals Company, were mixed together in a varying ratio by weight as shown in

Table 3
CYTOP concentration by weight percentage for various pore size electrodes.

Pore diameter (μm)	Aspect ratio (L/D)	CYTOP concentration (wt. %)
38	10	0.95
50	8	1.1
76	5	1.42
100	4	1.72

Table 3. The CYTOP concentrations were determined for the aspect ratio of our samples in reference to a similar work by Kedzierski et al. [28]. The porous wafers were dip-coated in the fluoropolymer solution. The drying process of the dip-coated wafers included 10 s of vertical drain, 5 min of soft dry at 80 °C, and final dry for 12 min at 200 °C to ensure complete evaporation of the solvent. Both of the drying steps were performed with the wafer suspended 2 inches above the hot plate to prevent clogging of the pores. A small portion of the wafer was treated with hydrofluoric acid (HF) to remove the SiO_2 and CYTOP coating at that small location to expose a conductive contact to connect to a copper wire.

3.2. Measurement set-up

A custom-built measurement set-up for high surface area REWOD energy harvesting is illustrated in Fig. 4 (physical test set-up is shown in Fig. S3). It consisted of a subwoofer for generating pulsating pressure through vertical displacement of a syringe attached to the subwoofer. The syringe plunger was attached to a 3D printed stage that sits over the sub-woofer dust cap so that as the subwoofer moves up and down, the
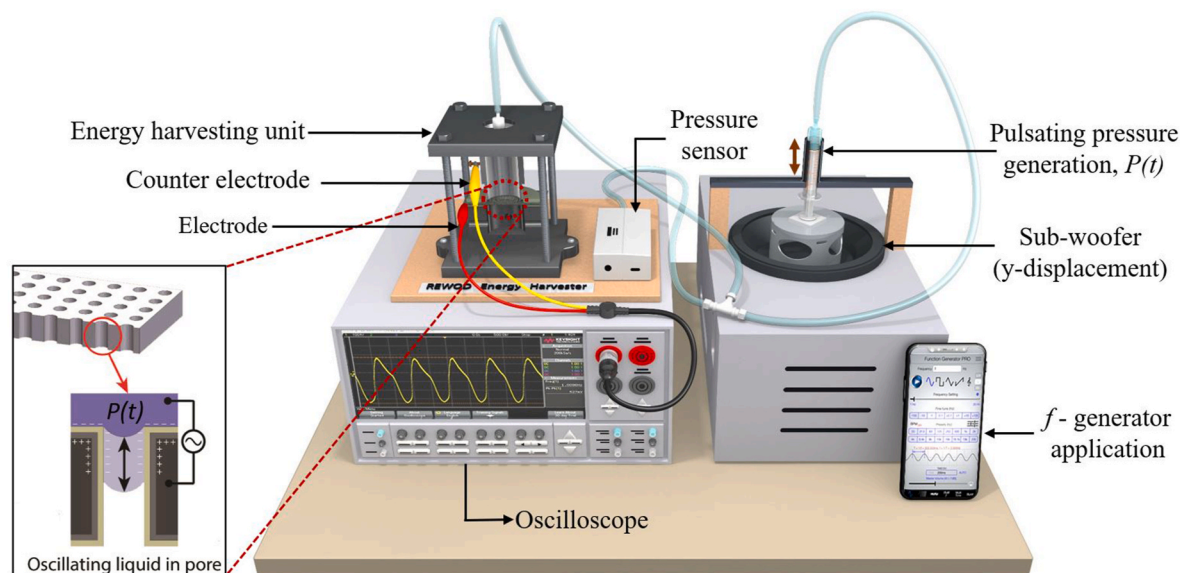
Fig. 4. (a) Measurement set-up of the high surface area REWOD energy harvesting. The inset shows pulsating pressure acting on a reservoir of electrolyte sitting on top of a porous electrode within an air-tight chamber.

syringe plunger moves along with it. The subwoofer was controlled by a signal generating mobile phone application (Audio Function Generator PRO). A communication cable from the subwoofer was connected to the audio jack of the mobile phone with the application to supply the sinusoidal signal at a given amplitude and frequency to produce modulating subwoofer vertical displacement. This signal output from the application excites the subwoofer to move up and down at a desired frequency and amplitude. The shaker system consisted of an 8-inch 800-W subwoofer (Pyle), a 400 W amplifier (Boss CX250), and a 12-V power source (Apevia ATX Raptor) attached to a power adapter cord. Similar custom-made systems have been reported in prior energy harvesting research [40–42]. This was a simple, inexpensive method for generating low-frequency and relatively high amplitude oscillations. A custom wood enclosure provided a location to mount the subwoofer and also contained the power amplifier and the DC power source.

The "System Volume" feature in the mobile application corresponds to the vertical displacement amplitude of the syringe plunger and hence the magnitude of the pressure generated. The pressure magnitude is higher for a higher frequency of oscillation at a fixed system volume. Pressure can be precisely controlled by adjusting the function generator amplitude for any given frequency in the application. Pulsating pressure generated in the form of sinusoidal peak-to-peak pressure for a frequency range of 1–5 Hz with 1 Hz step size for a range of system volumes were measured using a pressure sensor (PASCO PS-320). The measured pressure values were approximately within the range of 1.5–16 kPa and the results are summarized in Fig. S4. This range of pressure is well within the range of Laplace capillary pressure (discussed later in this section) required for the insertion and retraction of electrolyte in and out of pores for all pore geometry sizes in this work. The Laplace capillary pressure is the pressure that is required for liquid to penetrate into the micropores. The equation for this pressure is $P = 2\gamma cos\theta/r$ where γ is the surface tension between the electrolyte and the surrounding air, θ is the contact angle between the electrolyte and the CYTOP coating, and r is the pore radius. As an illustration, a representative sinusoidal pulsating pressure generated at 1 Hz frequency with a system volume of 65 is given in Fig. S5. Once the pulsating pressure generated by the subwoofer system reaches the capillary pressure at a given frequency, the liquid electrolyte is inserted into and retracted out of the pores. This liquid movement results in a periodically changing electrode-electrolyte interfacial area, which results in a periodic change in surface charge and therefore AC voltage/current.

The REWOD energy harvesting unit in Fig. 4 and also in Fig. S6 consisted of hollow upper and bottom chambers. The upper chamber is an aluminum housing and acts both as a counter electrode as well as an airtight compartment to prevent pressure leakage during experiments. The bottom housing is a 3D-printed PLA fixture to support the porous electrode. The electrode was cushioned and sealed on either side with silicone gaskets with the same circular area to that of the porous section of the electrodes (3.14 cm^2). Once the REWOD energy harvesting unit was securely set up then deionized (DI) water, which is used as an electrolyte in this work, was placed on the porous area of the electrode, AC voltage measurement using oscilloscope (Keysight InfiniiVision DSOX3014A) and RC measurement using AD5940 (an impedance and electrochemical front end by Analog Devices) were performed. DI water was used as an electrolyte so that it was easier to clean and dry the porous samples for multiple experiments.

Before the actual measurements of the AC voltage began, several trial AC voltage measurements were performed by applying pulsating pressure in small increments starting with a lower limit (~1.5 kPa) to observe any increase in the magnitude of the AC voltage. The optimum peak-to-peak pulsating pressures for all the pore size electrodes were determined experimentally in order to ensure there is neither excess pressure, causing electrolyte leakage from the bottom of the pores, nor is there insufficient pressure preventing electrolyte from contacting the entire pore walls. Applied pressure from the pulsating pressure device was gradually increased to realize a proportional increase in the magnitude of the AC voltage until the AC signal magnitudes dropped close to zero from the oscilloscope indicating electrolyte leakage beneath the porous electrode. The pressure right before the lamented signal was adopted as the optimum peak-to-peak pressure required for maximum electrode-electrolyte interfacial area and hence the maximum AC voltage generation. The process was repeated for all four pore sizes and the relevant peak-to-peak pressures were recorded. Theoretical capillary pressure as given by the Laplace capillary pressure equation where $\gamma = 0.072$ N/m and $\theta = 110°$ were calculated for all pore sizes in this work. These parameters to calculate the capillary pressure were adopted from work by Han et al. [43]. Table 4 summarizes the Laplace pressure and actual applied pressure required for optimum insertion and retraction of electrolyte in and out of the pores for all pore sizes. In the table, the peak pressure, which is slightly higher than the Laplace pressure for each pore, is half of the applied (peak-to-peak) pulsating pressure. It only requires half the magnitude of the peak-to-peak

Table 4
Experimental and theoretical (Laplace) pressure required for optimum insertion and retraction of electrolyte in and out of pores for all pore size electrodes during modulation.

Pore diameter (μm)	Laplace pressure (kPa)	Applied peak pressure (kPa)	Error (%)
38	2.60	2.8	7.2
50	1.98	2.1	5.9
76	1.30	1.4	7.2
100	0.99	1.1	10.2

pressure to either insert or retract the electrolyte into or out of the pores. The error percentage ranges from 7.2 to 10.2%, which is the percentage difference between the peak pressure and the Laplace pressure, and could be attributed to liquid pinning effects and slight air leakage in the experimental set-up and during the measurements. A representative plot of both the Laplace and experimental peak pressure with respect to the pore radius is given in Fig. S7. The close agreement of Laplace pressure and actual pressure is important because it provides verification that the electrolyte fills the pores, which is something that cannot be visually observed in our test set-up.

4. Results and discussion

4.1. AC voltage measurement

AC voltage generation in REWOD is the direct result of periodically changing electrode-electrolyte interfacial area from an externally applied pulsating pressure, which forms a time-varying electrical double layer (EDL) capacitance. EDL capacitance is formed due to the polarization of opposite charges at the interface between the electrode and the electrolyte. The capacitance at the electrode-electrolyte interface in REWOD is the result of the capacitance from the EDL at both the uninsulated top (aluminum housing) and the insulted bottom electrode. However, because the capacitance at the uninsulated electrode is much larger ($C = \varepsilon A/d$, $d_{bare} \ll d_{insulated}$), it is therefore neglected in this work because its contribution to total capacitance is negligible when in series with the capacitance at the insulated electrode. The capacitance at the dielectric insulator is modeled as a simple capacitor with SiO$_2$/CYTOP as dielectric in between the two conductive media (the very low resistance Si-wafer and the electrolyte).

AC voltages for each pore size were measured for a frequency range of 1–5 Hz with 0.5 Hz step size using an oscilloscope (Keysight Infin-iiVision DSOX3014A). AC voltage increases with increasing frequency showing almost a linear relationship between the voltage and the

frequency. Increasing oscillation frequency increases the dynamics of the electrical charge transfer per unit time during the REWOD process resulting in a higher current ($i = dQ/dt$). Considering constant resistance, increasing current also increases the voltage according to Ohm's law. AC voltage is higher for smaller pores as expected based on the total surface area and the corresponding capacitance. Fig. 5(a) shows the peak-to-peak AC voltage (V_{P-P}) for all pore sizes with respect to frequency (Hz). Each measurement result is presented with an error bar representing $+/-$ one standard deviation from the mean of three measured results. A representative plot of measured AC voltage vs. time over a 3 s time period for the 38 μm pore size electrode at 3.0 Hz is shown in Fig. 5(b). From the figure, it can be observed that the voltage signal has 0.17 V of DC offset (difference between the maximum positive and negative peak) and a peak-to-peak amplitude of 2.4 V. Additional representative plots of measured AC voltage vs. time over a 3-s time period for the remaining pore sizes at 3.0 Hz are given in Figs. S8- S10. The magnitude of the AC voltage from this work is significant realizing that no bias voltage has been applied in the experiment. Among the representative AC peak-to peak voltage plots, there is a range of DC offsets as evidenced by the difference between positive and negative peaks. Although the experiments were performed with high precision, the DC offsets for various pore size electrodes at different frequencies ranged from 10 mV to 430 mV but the DC offset was independent of frequency. In order to demonstrate the variations of the DC offset voltage, the DC offset voltages for all four electrodes and nine frequencies of modulation are summarized as presented in Table S2. The DC offsets that are observed are primarily attributed to the constant portion of the capacitance (C_C). For example, referring to Table 2, the constant capacitance that contributes to the DC offset in peak-to-peak AC voltage range from 36 to 39 nF. Mathematically, the occurrence of DC offset voltage in REWOD can be described as follows: With reference to Fig. 2(a) in the design and theoretical modeling section, the charge, Q, across the capacitor (C_C) during oscillation is: $Q = C_C V_{out-DC}$, where $Q = \int i_{C_C}(t).dt$, yielding the relationship as given by Equation (5) between the constant portion of the capacitance (C_C) and the voltage output in the form of DC offset.

$$V_{out-DC} = \frac{1}{C_C} \int i_{C_C}(t).dt \tag{5}$$

4.2. RC measurements

In the modeled REWOD energy harvester with R_P and C_P in parallel with $I_P(t)$ as a current source originating from the REWOD, $C_P(t)$ acts as a variable capacitor that changes periodically during the electrolyte modulation while electrical resistance, R_P, occurs across the electrodes
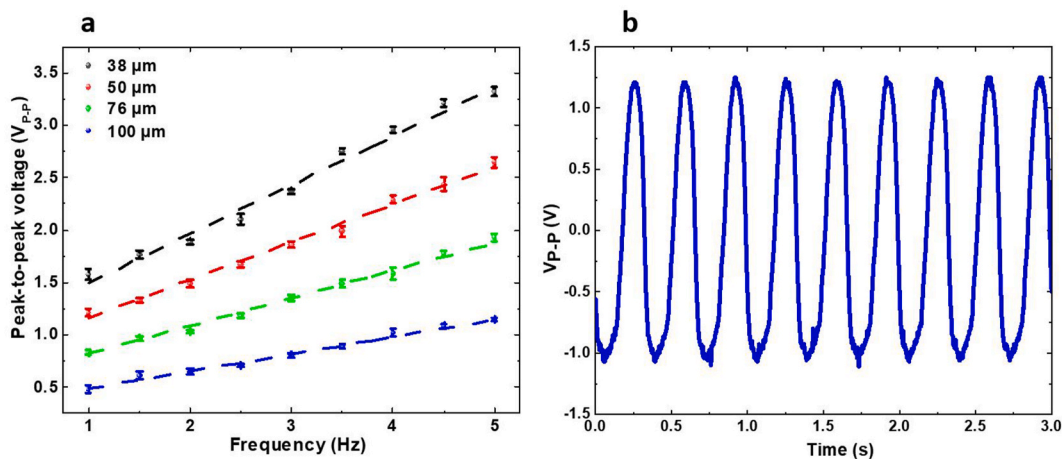
Fig. 5. (a) AC voltage with respect to frequency for all four pore size electrodes (dashed straight lines represent a linear fit of the data with error bars representing $+$/$-$ one standard deviation from the mean). (b) A representative AC voltage signal at 3.0 Hz frequency for an electrode with 38 μm pores during the first 3 s.

due to the electrical conductivity and thicknesses of the electrolyte, dielectric, and the conductive layers along with the electrode-electrolyte interfacial area. The R_P and $C_P(t)$ were measured during modulation using an impedance and electrochemical front end (AD5940) by Analog Devices. An image of the device is given in Fig. S11. This measurement provided the total impedance of the system and phase angle for any given frequency of oscillation. For R_P and C_P in parallel, the equivalent impedance is given by Equation (6). The resistance, R_P, is obtained by rearranging the equation for phase angle (Equation (7)). The equation for capacitance (Equation (8)) results from substituting Equation (7) into Equation (6) and solving for $C_P(t)$.

$$|Z| = \frac{1}{\sqrt{\left(\frac{1}{R_P}\right)^2 + (\omega C_P(t))^2}} \tag{6}$$

$$R_P = \frac{\tan(\varphi)}{-\omega C_P(t)} \tag{7}$$

$$C_P(t) = \frac{\tan(\varphi)}{\omega |Z| \sqrt{1 + \tan^2\varphi}} \tag{8}$$

In the above equations, $|Z|$ is the absolute impedance, φ is the phase angle, and $\omega = 2\pi f$ is the angular frequency of the AC signal where f is the applied frequency of oscillation. R_P and C_P for all four pore sizes were computed from the measured impedance and phase angle for a frequency range of 1–5 Hz with 0.5 Hz step size. Computed R_P results as shown in Fig. 6(a) suggest that the change in resistance either with pore size or the frequency was small. Additionally, there was no specific trend to the magnitude of R_P with the pore size or the frequency. The relatively constant R_P may be explained by examining Equations (7) and (8). Referring to Equation (8), capacitance decreases with increasing frequency. Similarly, referring to Equation (7), an increase in frequency offsets the decrease in capacitance in the denominator potentially resulting in a nearly constant R_P. Fig. 6(b) shows the total measured capacitance densities for all the pore sizes and oscillation frequencies used in this work. Capacitance decreased with increasing frequency for all pore sizes validating the relationship in Equation (8).

AC current was computed from the measured values of AC voltage (V_{AC}) and impedance ($|Z|$) using Ohm's law ($I = V_{AC}/|Z|$). The magnitude of the current with respect to frequency follows the same pattern as that of AC voltage (Fig. 5(a)) since the impedance for a given pore size remained fairly constant. Fig. 7(a) shows the peak-to-peak AC current for all pore sizes with respect to frequency. Each computed result is presented with an error bar representing $+/-$ one standard deviation from the mean of three computed results. A representative plot of AC

current vs. time for a 38 μm pore size electrode at 3.0 Hz frequency is shown in Fig. 7(b). From the figure, it can be observed that the AC current has 0.5 μA of DC offset (difference between the maximum positive and negative peak) and 8.4 μA of peak-to-peak amplitude. In accordance with the voltage vs. frequency, the AC current also shows almost a linear relationship between the oscillation frequency and the peak-to-peak AC current. Current also increases with shrinking pore size, which is purely due to the fact that the surface area increases with decreasing pore size. The maximum current of 11.83 μA for the total planar area of 3.14 cm² was generated using an electrode containing 38 μm-diameter pores at 5 Hz frequency, which corresponds to 3.77 μA/cm² of current density. The lowest current density was 0.6 μA/cm² and was obtained with an electrode containing 100 μm-diameter pores at 1 Hz oscillation frequency.

The current densities presented here are more dependent on total electrode-electrolyte interfacial area than the pore size. The electrodes were fabricated to ensure that there is sufficient area between each pore to prevent breakage due to the fragile nature of the silicon wafers. Only a fraction of the 3.14 cm² wafer area was used for pores. Referring to Table 1, only up to 0.59 cm² of the 3.14 cm² circular area was used for pores which is ~19% of the total available surface area. Since the capacitance and the resulting AC voltage/current are proportionally dependent on electrode-electrolyte interfacial area, more pores could be created to increase the power output. Presumably, if the pores were increased 3 times to cover ~57% of the total available surface area, power output could have been increased by 3 times although with a compromise in substrate strength.

A comparison between measured and theoretical capacitance is presented in Table S3. Measured capacitances are higher by as much as 35% compared to the theoretical capacitances calculated using Equation (1). SEM images (Fig. S12) reveal that the pores after DRIE were extremely rough. The higher measured capacitance is attributed to the roughness of the electrodes and therefore much higher surface area. Since the capacitance (C) is proportional to the electrode-electrolyte interfacial area (A), higher surface area contributed to the higher measured capacitance. In addition, the parasitic capacitance from the cables and connectors may also have contributed to the higher measured capacitance. Fig. 8(a) shows a comparison between the theoretical and measured capacitance densities for all pore sizes at 1 Hz oscillation frequency. A representative plot of measured capacitance density vs. time for a 38 μm diameter pore electrode at 1 Hz frequency is given in Fig. S13.

The maximum power can be harvested when the source impedance of the REWOD ($|Z_S|$) is matched with an optimal external load. Considering an optimal load such that $|Z_S| = |Z_L|$, the root mean square
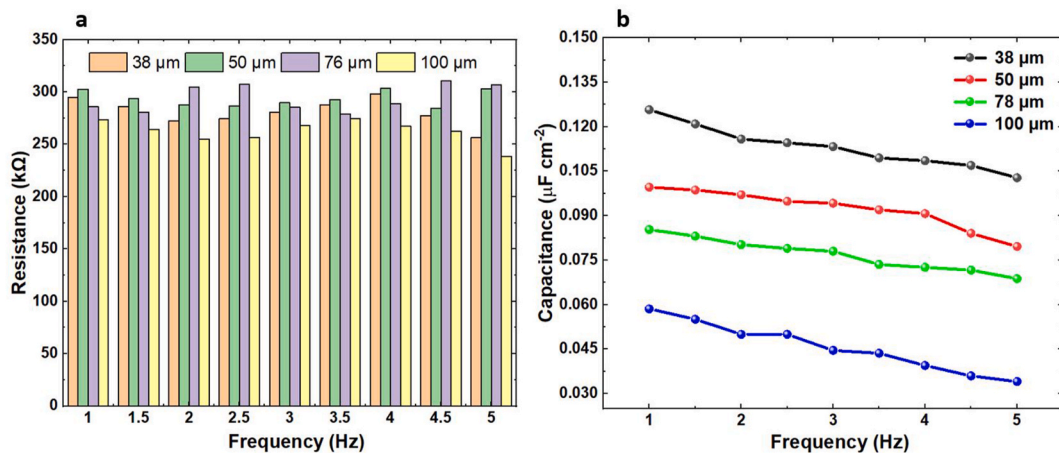

Fig. 6. (a) Computed resistances for 38 μm, 50 μm, 76 μm, and 100 μm diameter pores for a frequency range of 1–5 Hz with 0.5 Hz step. (b) Measured capacitance densities for 38 μm, 50 μm, 76 μm, and 100 μm diameter pores for a frequency range of 1–5 Hz with 0.5 Hz step.
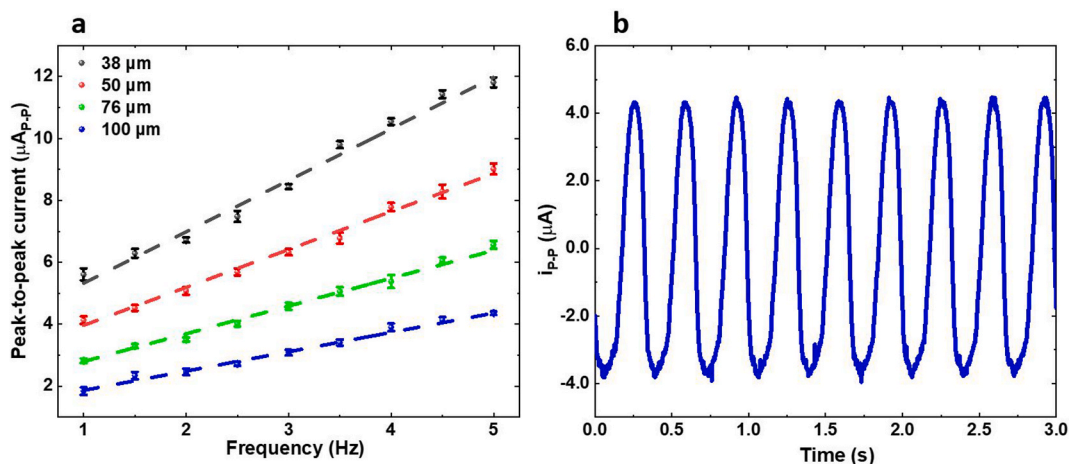
Fig. 7. (a) AC current with respect to frequency for all four pore size electrodes (dashed straight lines represent a linear fit of the data with error bars representing + /− one standard deviation from the mean). (b) A representative AC current signal at 3.0 Hz frequency for an electrode with 38 μm pores during the first 3 s.
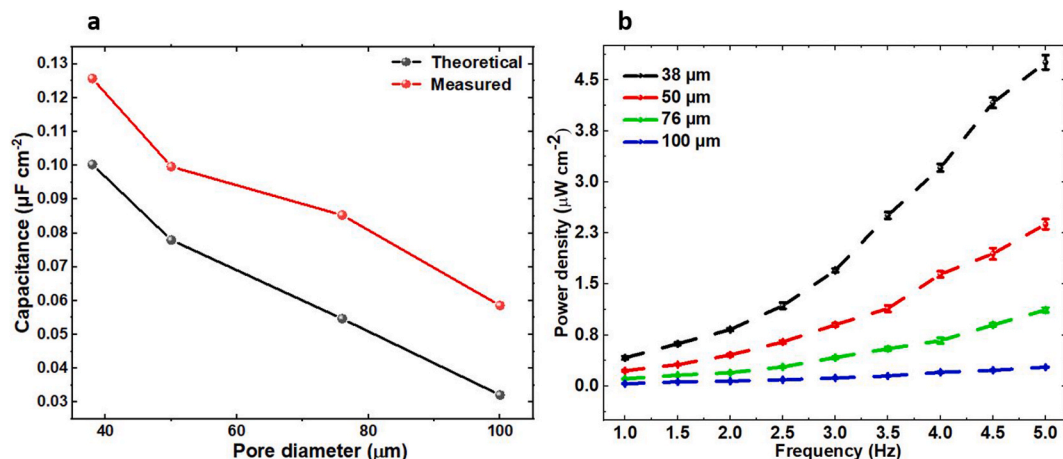

Fig. 8. (a) Theoretical and measured capacitance densities for all pore sizes at 1 Hz frequency. (b) Power density of the REWOD energy harvester without an optimal load with respect to increasing frequency and shrinking pore size (data is presented with error bars representing + /− one standard deviation from the mean).

(RMS) power density is calculated using Equation (9):

$$P_{RMS} = \frac{V_{RMS}^2}{4|Z_L|A} \tag{9}$$

where V_{RMS} is the RMS voltage, $|Z_L|$ is an optimal external load, and A is the electrode-electrolyte interfacial area. Using RMS voltage of 1.175 V for a 38 μm pore electrode at 5 Hz oscillation frequency, calculated based on Fig. 5(a), and the corresponding impedance calculated based on resistance of 257 kΩ from Fig. 6(a), the RMS power with an optimal load is calculated to be 3.75 μW for the given planar area of 3.14 cm² which corresponds to 1.2 μW/cm² of power density. Considering a voltage source of magnitude ($V_{RMS-open}$) and an internal source impedance $|Z_S|$, the voltage is divided by half when actually harvesting on the optimal load $|Z_L|$. Therefore, without an optimal load, the power density increases four times to 4.8 μW/cm² as supported by Equation (9).

One of the objectives of this work is to study how frequency and electrode pore size affect output power and thus the power density. RMS power densities for all pore size electrodes at all the modulation frequencies are calculated and presented in Fig. 8(b). From the figure, it is observed that the power density increases with increasing frequency and shrinking pore size. Increase in power density with increasing frequency is in accordance with increase in voltage and current with increasing frequency since power is directly proportional to the voltage and the current. Likewise, increase in power density with shrinking pore size is

primarily attributed to increasing electrode surface area with decrease in pore sizes. Power conversion efficiency from this work is determined to be 6.04%. A complete power conversion efficiency derivation with calculation is provided in the supplementary information section S1. Despite low power conversion efficiency, power density from this work is very well enhanced from our previous work on planar electrodes (~23 times) and could be further improved considering a higher surface area material such as denser pores or conductive porous carbon materials [20]. Considering the absence of bias voltage and the proposed avenue to enhance the AC voltage generation, bias-free REWOD energy harvesting using high surface area materials could successfully lead to fully self -powered wearable motion sensors for applications such as wearable human health monitoring in real time.

5. Conclusion

REWOD energy harvesting using high surface area porous electrodes with uniform pores was performed with an objective of generating high power density output without any external bias source. Four different pore-diameter electrodes, 38 μm, 50 μm, 76 μm, and 100 μm, were fabricated on Si wafers with a fixed thickness. Understanding the aspects of capillary pressure was essential for complete insertion and retraction of electrolyte in and out of pores to generate maximum capacitance and maximum power output. Without any external DC bias voltage, AC

voltage was generated and AC current was determined by computing R_P and C_P using a parallel configuration model and the results were validated through experimental measurements. The maximum voltage density was measured to be 1.05 V/cm^2 and the maximum current density was computed to be 3.77 μA/cm^2. The power density with optimal load was 1.2 μW/cm^2 and without load the power density was 4.8 μW/cm^2. Power density from this work is very well enhanced to as high as ~23 times from our previous work on planar electrodes and could be further improved considering a higher surface area material such as one with denser pores or conductive porous carbon materials. Considering the absence of bias voltage and the proposed avenue to enhance the AC voltage generation, bias-free REWOD energy harvesting using high surface area materials could successfully lead to fully self-powered wearable motion sensors or other applications requiring a reliable, compact, and long-term power source.

CRediT authorship contribution statement

Pashupati R. Adhikari: Conceptualization, Methodology, Investigation, Materials fabrication and characterization, Experimental measurements, Data curation, Visualization, Manuscript writing. **Russell C. Reid:** Conceptualization, Validation, Investigation, Visualization, Supervision, Funding acquisition. **Ifana Mahbub:** Validation, Investigation, Visualization, Supervision, Funding acquisition, All authors reviewed manuscript.

Declaration of competing interest

The authors declare that they have no known competing financial interests or personal relationships that could have appeared to influence the work reported in this paper.

Acknowledgments

Appendix A. Supplementary data

Supplementary data to this article can be found online at https://doi.org/10.1016/j.jpowsour.2021.230726.

References

[1] T. Krupenkin, J.A. Taylor, Reverse electrowetting as a new approach to high-power energy harvesting, Nat. Commun. 2 (2011) 448.

[2] T.-H. Hsu, J.A. Taylor, T.N. Krupenkin, Energy harvesting from aperiodic low-frequency motion using reverse electrowetting, Faraday Discuss 199 (2017) 377–392.

[3] F.U. Khan, M.U. Qadir, State-of-the-art in vibration-based electrostatic energy harvesting, J. Micromech. Microeng. 26 (2016) 103001.

[4] D.-A. Wang, K.-H. Chang, Electromagnetic energy harvesting from flow induced vibration, Microelectron. J. 41 (2010) 356–364.

[5] Y. Zhang, A. Luo, Y. Wang, X. Dai, Y. Lu, F. Wang, Rotational electromagnetic energy harvester for human motion application at low frequency, Appl. Phys. Lett. 116 (5) (2020), 053902.

[6] Y. Peng, et al., An efficient piezoelectric energy harvesting interface circuit using a sense-and-set rectifier, IEEE J. Solid State Circ. 54 (2019) 3348–3361.

[7] F. Xing, Y. Jie, X. Cao, T. Li, N. Wang, Natural triboelectric nanogenerator based on soles for harvesting low-frequency walking energy, Nano Energy 42 (2017) 138–142.

[8] A. Pachi, T. Ji, Frequency and velocity of people walking, Struct. Eng. 83 (2005) 36–40.

[9] J. Chen, Z.L. Wang, Reviving vibration energy harvesting and self-powered sensing by a triboelectric nanogenerator, Joule 1 (2017) 480–521.

[10] N. Cui, et al., Dynamic behavior of the triboelectric charges and structural optimization of the friction layer for a triboelectric nanogenerator, ACS Nano 10 (2016) 6131–6138.

[11] Z. Zhang, K. Du, X. Chen, C. Xue, K. Wang, An air-cushion triboelectric nanogenerator integrated with stretchable electrode for human-motion energy harvesting and monitoring, Nano Energy 53 (2018) 108–115.

[12] C. Wang, S.-K. Lai, Z.-C. Wang, J.-M. Wang, W. Yang, Y.-Q. Ni, A low-frequency, broadband and tri-hybrid energy harvester with septuple-stable nonlinearity-enhanced mechanical frequency up-conversion mechanism for powering portable electronics, Nano Energy 64 (2019) 103943.

[13] H. Yang, S. Hong, B. Koo, D. Lee, Y.-B. Kim, High-performance reverse electrowetting energy harvesting using atomic-layer-deposited dielectric film, Nano Energy 31 (2017) 450–455.

[14] J.K. Moon, J. Jeong, D. Lee, H.K. Pak, Electrical power generation by mechanically modulating electrical double layers, Nat. Commun. 4 (2013) 1–6.

[15] H. Yang, H. Lee, Y. Lim, M. Christy, Y.-B. Kim, Laminated structure of Al_2O_3 and TiO_2 for enhancing performance of reverse electrowetting-on-dielectric energy harvesting, Int. J. Precis. Eng. Manuf-Green Technol. 8 (2019) 103–111.

[16] M. Zhu, F. Zhu, O.G. Schmidt, Nano energy for miniaturized systems, Nano Mater. Sci. (2020) 1–6.

[17] Z. Li, Q. Zheng, Z.L. Wang, Z. Li, Nanogenerator-based self-powered sensors for wearable and implantable electronics, Research (2020).

[18] A. Tricoli, N. Nasiri, S. De, Wearable and miniaturized sensor technologies for personalized and preventive medicine, Adv. Funct. Mater. 27 (2017) 1605271.

[19] R.C. Reid, I. Mahbub, Wearable self-powered biosensors, Curr. Opin. Electrochem. 19 (2020) 55–62.

[20] P.R. Adhikari, N.T. Tasneem, R.C. Reid, I. Mahbub, Electrode and electrolyte configurations for low frequency motion energy harvesting based on reverse electrowetting, Sci. Rep. 11 (2021) 5030.

[21] J. Yu, E. Ma, T. Ma, Harvesting energy from low-frequency excitations through alternate contacts between water and two dielectric materials, Sci. Rep. 7 (2017) 17145.

[22] L.E. Helseth, X.D. Guo, Contact electrification and energy harvesting using periodically contacted and squeezed water droplets, Langmuir 31 (2015) 3269–3276.

[23] T.-H. Hsu, J.A. Taylor, T.N. Krupenkin, Energy harvesting from aperiodic low-frequency motion using reverse electrowetting, Faraday Discuss 199 (2017) 377–392.

[24] T.-H. Hsu, S. Manakasettharn, J.A. Taylor, T. Krupenkin, Bubbler: a novel ultra-high power density energy harvesting method based on reverse electrowetting, Sci. Rep. 5 (2015) 16537.

[25] A.B. Kolomeisky, A.A. Kornyshev, Current-generating 'double layer shoe' with a porous sole, J. Phys. Condens. Matter 28 (2016) 464009.

[26] E.W. Washburn, The dynamics of capillary flow, Phys. Rev. 17 (1921) 273–283.

[27] M.W.J. Prins, Fluid control in multichannel structures by electrocapillary pressure, Science 291 (2001) 277–280.

[28] J. Kedzierski, K. Meng, T. Thorsen, R. Cabrera, S. Berry, Microhydraulic electrowetting actuators, J. Microelectromech. Syst. 25 (2016) 394–400.

[29] N.T. Tasneem, P.R. Adhikari, D.K. Biswas, R.C. Reid, I. Mahbub, Design of a reverse-electrowetting transducer based wireless self-powered motion sensor, in: IEEE International Symposium on Circuits and Systems (ISCAS), 2020, pp. 1–5.

[30] N.T. Tasneem, D.K. Biswas, I. Mahbub, P.R. Adhikari, R. Reid, Self-powered motion tracking sensor integrated with low-power CMOS circuitry, in: EEE International Symposium on Circuits and Systems (ISCAS), 2021, pp. 1–5.

[31] P.R. Adhikari, N.T. Tasneem, D.K. Biswas, R.C. Reid, I. Mahbub, Reverse electrowetting-on-dielectric energy harvesting integrated with charge amplifier and rectifier for self-powered motion sensors, in: ASME 2020 Int. Mech. Eng. Congr. Expo., 2020.

[32] H. Yao, Y. Liao, A.R. Lingley, A. Afanasiev, I. Lahdesmaki, B.P. Otis, B.A. Parviz, A contact lens with integrated telecommunication circuit and sensors for wireless and continuous tear glucose monitoring, J. Micromech. Microeng. 22 (7) (2012), 075007.

[33] Y.-T. Liao, H. Yao, A. Lingley, B. Parviz, B.P. Otis, A 3 μW CMOS glucose sensor for wireless contact-lens tear glucose monitoring, IEEE J. Solid State Circ. 47 (1) (2012) 335–344.

[34] E.Y. Chow, A.L. Chlebowski, P.P. Irazoqui, A miniature-implantable rf-wireless active glaucoma intraocular pressure monitor, IEEE Trans. Biomed. Circuits Syst. 4 (6) (2010) 340–349.

[35] Ç. Varel, Y.-C. Shih, B.P. Otis, T.S. Shen, K.F. Böhringer, A wireless intraocular pressure monitoring device with a solder-filled microchannel antenna, J. Micromech. Microeng. 24 (4) (2014), 045012.

[36] Y.J. Yoon, B. Kim, A new formula for effective dielectric constant in multi-dielectric layer microstrip structure, in: IEEE 9th Topical Meeting on Electrical Performance of Electronic Packaging 0(Cat. No.00TH8524), 2000, pp. 163–167.

[37] J. Robertson, High dielectric constant gate oxides for metal oxide Si transistors, Rep. Prog. Phys. 69 (2005) 327–396.

[38] D. Kumar, P. Chaturvedi, N. Jejurikar, Piezoelectric energy harvester design and power conditioning, in: 2014 IEEE Students' Conference on Electrical, Electronics and Computer Science, 2014, pp. 1–6.

[39] S.A. Pullano, I. Mahbub, S.K. Islam, A.S. Fiorillo, PVDF sensor stimulated by infrared radiation for temperature monitoring in microfluidic devices, Sensors 17 (2017) 850.

[40] D.H. Litwhiler, A Custom Vibration Test Fixture Using a Subwoofer, Proceedings of the 2011 IAJC-ASEE International Conference, 2011, pp. 1–11.

[41] T. Perera, S.A.C. Yohanandan, H.J. McDermott, A simple and inexpensive test-rig for evaluating the performance of motion sensors used in movement disorders research, Med. Biol. Eng. Comput. 54 (2016) 333–339.

[42] A. Nammari, L. Caskey, J. Negrete, H. Bardaweel, Fabrication and characterization of non-resonant magneto-mechanical low-frequency vibration energy harvester, Mech. Syst. Signal Process. 102 (2018) 298–311.

[43] K. Han, O.E. Woghiren, R. Priefer, Surface tension examination of various liquid oral, nasal, and ophthalmic dosage forms, Chem. Cent. J. 10 (2016) 31.